Journal of Power Sources 421 (2019) 132–138

Contents lists available at ScienceDirect

Journal of Power Sources

journal homepage: www.elsevier.com/locate/jpowsour

Rational design of multi-functional CoS@rGO composite for performance enhanced Li-S cathode

Cong Gao[a], Chuanzhen Fang[a], Haimin Zhao[b], Jiayi Yang[a], Zhida Gu[a], Wei Sun[b], Weina Zhang[a], Sheng Li[a,**], Li-Chun Xu[c,***], Xiuyan Li[c], Fengwei Huo[a,*]

[a] Key Laboratory of Flexible Electronics (KLOFE), Institute of Advanced Materials (IAM), Nanjing Tech University (NanjingTech), 30 South Puzhu Road, Nanjing, 211816, China
[b] Zhejiang Tianneng Energy Technology Co., Ltd, 18 Baoqiao Road, Huaxi Industrial Function Zone, Huzhou, 313100, PR China
[c] College of Physics and Optoelectronics, Taiyuan University of Technology, Taiyuan, 030024, China

HIGHLIGHTS

- CoS@rGO host has abundant polar adsorption sites to suppress polysulfides shuttle.
- CoS as catalyst could promotes the kinetics of polysulfides conversion.
- rGO can enhance the conductivity of electrode and prevent the aggregation of CoS.
- Trifunctional host can lower the self-discharge behavior of Li–S batteries.

GRAPHICAL ABSTRACT

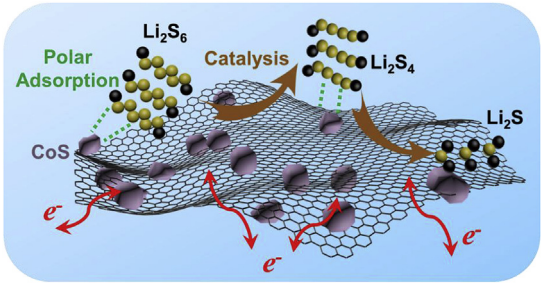

ARTICLE INFO

Keywords:
Catalytic
Polar
Conductive
Sulfur cathode
Self-discharge
Li-S battery

ABSTRACT

Lithium–sulfur battery has drawn widely attention due to its high theoretical energy density, in addition to the abundant and affordable sulfur. However, the battery performances are still not satisfied due to the undesired shuttle effect of polysulfides, the sluggish reaction kinetics, together with the intrinsic non-conductivity of active materials. Thus, the preparation of sulfur host materials with polar, catalytic and conductive properties can be an effective tactics. In this work, a cobalt sulfide@reduced graphene oxide composite has been designed and synthesized by a facile method, in which the CoS nanoparticles can provide more polar and catalytic sites to adsorb the polysulfides and accelerate the kinetics of polysulfides conversion. The rGO can serve as composite skeleton that could not only enhance the conductivity of electrodes, but also provide a sheet structure, preventing the aggregation of CoS nanoparticles. Moreover, the C–S bonds between CoS and carbon can further promote charge transfer and stabilize the composite. Benefiting from the trifunctional sulfur-host, the as-prepared cathode exhibits low self-discharge, good cycling stability and high rate performance for 602.0 mAh g^{-1} at 2 C. This sulfur-host design can be considered an effective and simple strategy for advanced Li-S battery.

* Corresponding author.
** Corresponding author.
*** Corresponding author.
E-mail addresses: iamsli@njtech.edu.cn (S. Li), xulichun@tyut.edu.cn (L.-C. Xu), iamfwhuo@njtech.edu.cn (F. Huo).

https://doi.org/10.1016/j.jpowsour.2019.03.015
Received 17 January 2019; Received in revised form 4 March 2019; Accepted 5 March 2019
0378-7753/

1. Introduction

The practical applications of traditional Li-ion batteries are limited by their energy density (400 Wh kg^{-1}), as both the burgeoning large-scale energy storage and electric vehicles technologies require high energy density [1,2]. Benefiting from the high theoretical energy density (2600 Wh kg^{-1}) and theoretical specific capacity (1675 mAh g^{-1}), Li–S batteries are considered as a promising candidate to meet growing demands of these technologies [3,4]. However, the commercialization of Li–S batteries is still impeded by the following three major challenges: 1) the soluble intermediate polysulfides (Li_2S_x, $4 \le x \le 8$) in the organic electrolyte can migrate between cathode and anode due to the concentration difference, leading to severe self-discharge behavior [5,6]; 2) the active material S and the final discharge products of lithium sulfides (Li_2S/Li_2S_2) are non-conductive, leading to a low utilization of active material and sluggish redox kinetics [7]; 3) the volumetric expansion from S (2.36 g cm^{-3}) to Li_2S (1.66 g cm^{-3}) is severe (about 80%), resulting in the pulverization of cathode and detachment from the current collector [8,9]. These problems give rise to the irreversible loss of active material S, poor Coulombic efficiency and the fast capacity decay.

Researchers have spent a great amount of time and efforts to address the above-mentioned limitations from various aspects, including the cathode modifications [10–12], the preparation of multi-functional separators [13–16], the usage of multi-functional binders [17–20] and new electrolyte systems [21–23]. Among these strategies, infiltrating sulfur into conductive porous materials has been an effective strategy in the past a few years, which can improve the electrochemical performance of cathode directly.

Carbonaceous materials, such as porous carbon [24,25], hollow carbon spheres [26,27], carbon nanotube [28] and graphene [29,30], have been widely explored as sulfur host due to their high conductivity, high porosity and adjustable surface properties, which could significantly improve the electrochemical performances of Li–S batteries. Nevertheless, the interaction between non-polar carbon material and polar polysulfides are mostly provided by Van der Waals forces, which is not strong enough to suppress the diffusion of polysulfides. A more effective way is to introduce various materials with polarity as sulfur host into Li–S batteries. Transition metal compounds with intrinsic polar surfaces such as metal oxides [31,32], sulfides [31,33], carbides [34,35] and nitrides [36] have been widely used as host materials to adsorb polysulfides. It also should be noted that the catalytic phenomenon could be found from these transition mental compounds in Li–S battery, promoting reaction conversion kinetics of polysulfides [37]. Among them, metal sulfides have drawn much attention due to their strong sulfiphilic property [38] and catalytic activity for accelerating redox reaction kinetics of polysulfides and Li_2S_2/Li_2S [39]. For example, pyrite CoS_2, TiS_2 and FeS_2 have been used as host materials to suppress the shuttle effects by a strong polar-polar interaction [40–43]. However, most of the conductivity of these still need to be improved. Although remarkable results have been achieved, designing multi-function host material with abundant catalytic, polar sites and high electrical conductivity is still imperative for Li–S battery.

Based on the above considerations, we designed and synthesized a composite of CoS nano-particles attaching on rGO surface (CoS@rGO) as a trifunctional surface host through facile hydrothermal method. As shown in Fig. 1, first, the CoS nano-particles provide more polar sites that can statically adsorb polysulfides by strong polar–polar interaction, which was confirmed by first-principles calculations and experiments. Second, the CoS nano-particles as catalysts were well distributed on rGO substrate and accelerated the kinetics of polysulfides conversion, reducing the loss of active sulfur. In addition, the C–S chemical bonds between rGO and CoS can serve as fast and continuous electronic channel toward the interface between CoS and polysulfides, leading to high utilization of active sulfur. Benefiting from this trifunctional sulfur-host, the as-prepared cathode exhibited low self-discharge, good cycling stability, and high rate performance for 602.0 mAh g^{-1} at 2 C. This sulfur-host design could be considered an effective and simple strategy for advanced Li-S battery.

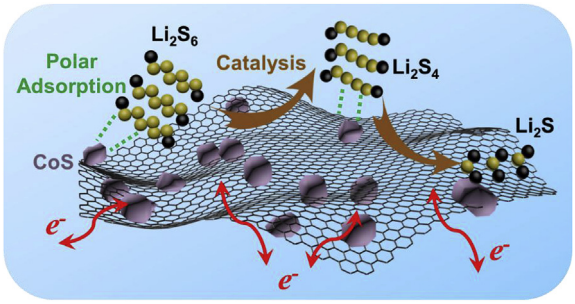

Fig. 1. Schematic illustration of roles played by the proposed CoS@rGO/S cathode during the discharge processes: adsorption of polysulfides, enhancement of the kinetics of polysulfides conversion by CoS catalyst and improved conductivity.

2. Experimental section

2.1. Synthesis of CoS@rGO, CoS and rGO

CoS@rGO composite was prepared by a facile hydrothermal method [44,45]. Briefly, 0.3425 g thiourea and 0.3736 g cobalt acetate tetrahydrate were added to 35 mL graphene oxide solution with a density of 3.43 mg mL^{-1} (GO, Tianjin Plannano Technology Co., Ltd) and dispersed by ultrasonic for 1 h. Then, the mixed solution was transferred into a Teflon autoclave (50 mL) and heated under 180 °C for 12 h. After it cooling down to room temperature, the black product was washed with deionized water and ethanol several times, and dried at 60 °C overnight.

The CoS sample was fabricated by the same process as CoS@rGO without adding GO.

The RGO sample was obtained by the heat treatment of GO at 180 °C for 12 h.

2.2. Preparation of CoS@rGO/S and other contrast samples

The CoS@rGO (or CoS, rGO) and sulfur powder with a mass ratio of 3:7 were ground in an agate mortar for 30 min. Then, these mixtures were transferred into Teflon autoclaves under an inert gas atmosphere and heated at 155 °C for 12 h to get the CoS@rGO/S (or CoS/S, rGO/S) composite.

2.3. Material characterization

The structure and morphology of the obtained samples was identified by a field-emission scanning electron microscopy (FESEM, JEOL, JSM-7800F) and a transmission electron microscopy (TEM, JEOL, JEM-2100F), installed with an Energy Dispersive Spectrometer (EDS, OXFORD). The HAADF-STEM image was collected by JEM-2100F field-emission TEM at 200 kV. The crystal structure of samples were identified by a X-ray diffractometer (XRD, SmartLab3Kw, Cu Kα radiation, λ = 1.5418 Å) at a scan rate of 20° min^{-1}. TGA was operated with METTLERTGA2 thermo analyzer under N_2 or O_2 atmosphere at a heating rate of 10 K min^{-1}. XPS analysis was tested by thermo scientific escalate 250XI and dealt with a CasaXPS software.

2.4. Electrochemical measurement

Homogeneous slurries were prepared by grinding 70 wt% active material, 20 wt% Super P and 10 wt% polyvinylidene fluoride (PVDF) in an agate mortar for 30 min. Then, the sulfur cathodes were fabricated

by putting slurry on the carbon-coated Al foils and vacuum drying under 60 °C for overnight. The electrodes were cut into circle with a diameter of 12.7 mm and mass loading was about 1–2 mg for per electrode. Half cells (CR2025) were assembled in an argon-filled glovebox under the content of O_2 and H_2O < 0.5 ppm, using polypropylene separator and Li anode. The electrolyte was brought from DoDochem, including 1 mol/L lithium bistrifluoromethanesulphonylimide (LiTFSI) and 0.2 mol/L lithium nitrate ($LiNO_3$) in a mixed solvent of 1,2-dimethoxyethane (DME) and 1,3-dioxolane (DOL) (v:v = 1:1). The electrochemical performances of Li–S batteries were tested on a LAND CT2001A battery systems. The CV curves and EIS curves were recorded by BioLogic Science Instruments. The cycle voltage window was from 1.8 V to 3.0 V.

The symmetric cells also were assembled by the process mentioned above, which with two same CoS@rGO (rGO) electrodes without active sulfur. Binder and every host material (CoS@rGO and rGO) with a mass ratio of 1:2 were mixed with NMP under stirring overnight. Then slurry was coated on carbon-coating Al foils as symmetric electrodes. These electrodes served as counter and working electrodes with 30 μL electrolyte including 0.8 M Li_2S_6 solution and the electrolyte of Li–S battery. The electrolyte of Li–S battery without Li_2S_6 served as a reference sample. CV profiles of symmetrical cells were recorded at a scan rate of 50 mV s^{-1}. EIS curves were tested at open circuit potential with a scanning frequency range from 10 mHz to 200 kHz.

2.5. Visualized adsorption experiment

Li_2S_6 solution was prepared by sulfur reaction with lithium sulfide (n:n = 5:1) in DME under 80 °C overnight. An appropriate amount of CoS@rGO powder was added to 2 mL Li_2S_6 solution (2 mM). By comparison, a blank experiment without CoS@rGO powder was carried out. All processes are carried out in an argon-filled glove box.

2.6. Density functional theory calculation

We studied the adsorption properties of the Li_2S_6 on CoS by the first-principles calculations within the density functional theory (DFT) [46]. The projector augmented wave (PAW) method [47–49] was employed, as implemented in the Vienna ab initio simulation package (VASP) [47]. The generalized gradient approximation (GGA) of Perdew-Burke-Ernzerhof (PBE) parameterization for the exchange and correlation functional was used [50]. The vacuum distance between CoS panels and their image is larger than 24 Å. The cell parameter is 12.32 × 13.47 Å for CoS (101) surface with 136 atom layers. A 5 × 5 × 1 grid for k-point sampling was employed and the value of the plane-wave energy cutoff was 400 eV. Good convergence was obtained with these parameters and the total energy was converged to 1.0×10^{-5} eV/atom.

3. Results and discussion

The morphology and structure of CoS and CoS@rGO are collected by scanning electron microscope (SEM) and transmission electron microscope (TEM). As shown in the images in Figs. S1a and S1b, the CoS sample without rGO is aggregated as sheets clusters, which has a size of about 5 μm. The SEM and TEM images of CoS@rGO composite (Fig. 2a and b) display the uniform attachment of CoS nano-particles on the rGO surface with a size of mainly ranging from 10 nm to 70 nm, which could also be evidenced in Fig. S2. The well distribution of the nano-particles could provide a relatively large surface area. Moreover, the high-resolution TEM image of CoS@rGO composite demonstrates a distinct lattice spacing of 0.25 nm (Fig. 2c and d) corresponding to the (101) plane of CoS. The high-angle annular dark-field scanning TEM (HAADF-STEM) is further performed to study the elemental composition and distribution of CoS@rGO composite (Fig. 2e). The related Energy-dispersive X-ray (EDX) spectroscopy furtherly confirm the uniform distributions of CoS nano-particles on rGO sheet (Fig. 2f–g). In addition,

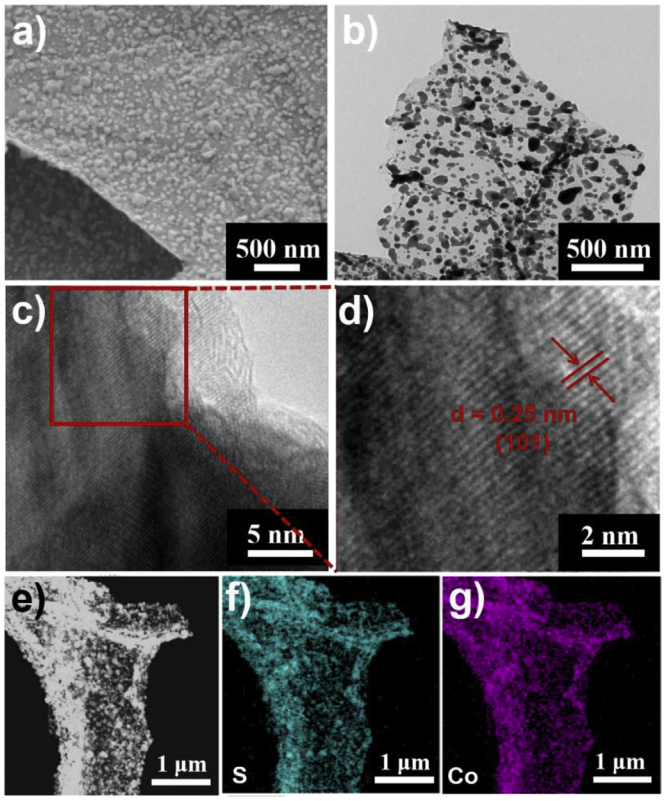

Fig. 2. a) SEM image of CoS@rGO. b) TEM image and c-d) high-resolution TEM (HRTEM) images of CoS@rGO. e-g) HAADF-STEM image and the corresponding EDS elemental mapping of S and Co.

the nitrogen adsorption/desorption behaviors of CoS@rGO (28.7 $m^2 g^{-1}$) in Fig. S3 present a much higher Brunauer-Emmett-Teller (BET) surface area than CoS (8.7 $m^2 g^{-1}$), proving that CoS@rGO composite could offer a large contact area between the active S material and the host, providing more catalytic and polar adsorption sites for polysulfides during electrochemical reactions.

X-ray diffraction (XRD) is employed to investigate the crystal structure of CoS@rGO and CoS@rGO/S composite (cathode composite after S incorporation). Fig. 3a demonstrates that the main characteristic peaks of as-prepared CoS and CoS@rGO are in good accordance with those of the simulated CoS (PDF 65–3418). It also reveals that the characteristic peaks of the obtained CoS/S and CoS@rGO/S composites are the combination of those of the S and CoS, indicating no side reaction during sample preparation (Fig. 3b).

Thermogravimetric analysis (TGA) is carried out to figure out the proportions of different components in the composite. After testing CoS@rGO composite in O_2 atmosphere at a rate of 10 °C min^{-1} from 30 °C to 600 °C, the CoS content in the composite is shown to lose within two temperature regions: 30–400 °C and 400–600 °C (Fig. 3c). The weight loss between 30 and 400 °C should be ascribed to the evaporation of moisture and partial oxidation reaction of rGO, while the weight loss in the other region relates to further oxidation reaction of rGO with O_2 and the conversion of CoS into Co_3O_4 [51]. According to the oxidation reaction of 3CoS (s) + 2O_2 (g) = Co_3O_4 (s) + 3S (g), the CoS and rGO contents in the CoS@rGO composite are calculated to be 68.9% and 31.1%, respectively. Moreover, in N_2 atmosphere, with a heating rate of 10 °C min^{-1}, the active sulfur content in CoS/S and CoS@rGO/S is confirmed as high as 70% (Fig. 3d).

The chemical state of CoS@rGO composite was then studied by X-ray photoelectron spectroscopy (XPS). Fig. 4a shows the survey XPS of CoS@rGO composite, demonstrating the co-existence of Co, O, C and S. Four peaks at 284.8, 286.2, 286.8 and 288.2 eV are evidently shown in

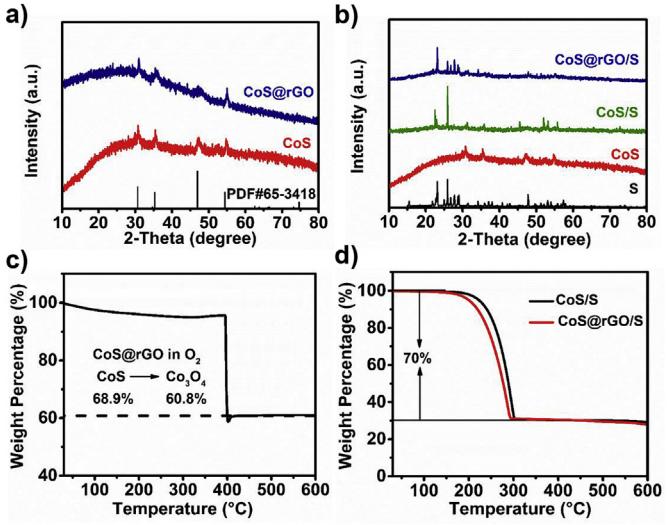

Fig. 3. a) XRD patterns of CoS, CoS@rGO and CoS standard reference. b) XRD patterns of S, CoS, CoS/S and CoS@rGO/S composites. c) TGA curve of CoS@rGO in O_2 atmosphere. d) TGA curves of CoS/S and CoS@rGO in N_2 atmosphere.

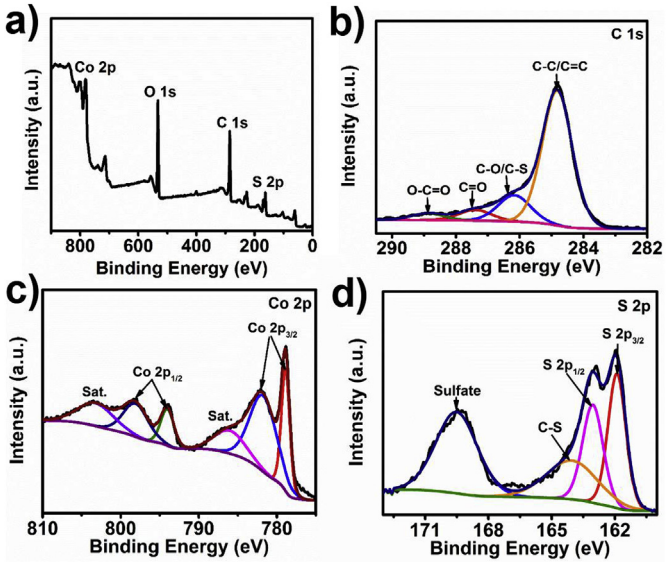

Fig. 4. (a) Survey XPS spectra of CoS@ rGO composite. High resolution XPS spectra of C 1s (b), Co 2p (c) and S 2p (d) for CoS@rGO composite.

the C 1s spectrum of the CoS@rGO composite (Fig. 4b), corresponding to C-C/C=C, C-O/C-S, C=O and O-C=O bonds, respectively [52–54]. The Co 2p spectrum (Fig. 4c) displays two doublets, corresponding to Co $2p_{1/2}$ and Co $2p_{3/2}$, respectively, which are in accordance with reported literature [54–56]. As shown in the S 2p spectrum in Fig. 4d, two peaks at 161.9 and 163.0 eV are ascribed to the S $2p_{3/2}$ and S $2p_{1/2}$ of CoS@rGO, respectively [56]. It is worth noting that the peak at 164.0 eV corresponds to C-S bond [54], indicating the in-situ growth and tight bonding of CoS nano-particles on the rGO surface. This bonding state of the CoS would provide strong polar adsorption between polysulfides and the host materials.

In order to prove the polar adsorption feature of CoS@rGO composite to polysulfides, a certain amount of CoS@rGO powder was added to 2 mM Li_2S_6 solution. Fig. 5a clearly shows that the color of Li_2S_6 solution with CoS@rGO changes from dark yellow to transparent clear after 5 h, while that of the blank Li_2S_6 solution remains dark yellow. Then, XPS analysis was performed on the CoS@rGO after the absorption (Fig. S4). Compared with the Co 2p spectrum of pure CoS@rGO, the peaks of CoS@rGO + Li_2S_6 had obviously shift which is in accordance with reported literature [54,57]. DFT calculations have also been employed to understand the interaction between CoS and lithium polysulfides (e.g. Li_2S_6) in Fig. 5b. The (101) surface of CoS was taken as an example to study the Li_2S_6 adsorption capability (Fig. 5b), which can be described by the binding energy (Eb): $Eb = E_{CoS\text{-}Li2S6} - E_{CoS} - E_{Li2S6}$, where $E_{CoS\text{-}Li2S6}$ represents the energy of the CoS (101) surface with Li_2S_6, E_{CoS} is the energy of the (101) surface of CoS and E_{Li2S6} stands for the energy of Li_2S_6. As calculated, the binding energy between the (101) surface of CoS and Li_2S_6 is −4.23 eV, indicating the strong adsorption capability of CoS [57–59]. The self-discharge behavior tests were further carried out. Fig. 5c shows that the voltage change of S and CoS@rGO/S electrodes before and after 1st cycle. The open circuit voltage of CoS@rGO/S electrode was almost not changed before and after one cycle, indicating it can limit the battery self-discharge. By comparison, the S electrode showed severe self-discharge behavior. Therefore, CoS@rGO as sulfur host can effectively suppress the polysulfides shuttle for Li–S batteries. Then electrochemical cycling performance was then tested with CoS@rGO/S electrodes to prove the polar adsorption effect of the host. As shown in Fig. 5d, the long-term cycling performance and its Coulombic efficiency of the sample were recorded. After running the first ten cycles at 0.1 C, the discharge specific capacity of CoS@rGO/S could achieve 806.2 mAh g^{-1} (based on sulfur weight) at a high current density of 1 C. After 200 cycles, a reversible discharge specific capacity of 570.0 mAh g^{-1} is still remained and a Coulombic efficiency of 99.5% is maintained. All of these results indicate that the introduction of CoS plays a key role in suppressing the shuttle effect leading to the electrochemical performance improvement of Li–S batteries. It should be explained that the reason of capacity decay is complex. It is related to the overall electrochemical of battery, not only the polysulfides shuttle effect, but also the Li anode and electrolyte. The side reaction between polysulfides and Li metal and the high reactivity of Li dendrite could facilitate the electrolyte decomposition, resulting in the capacity degradation.

The cyclic voltammetry (CV) is performed to evaluate the catalytic effect of CoS [60]. CoS@rGO and rGO electrodes without active sulfur served as symmetric electrodes are assembled with Li_2S_6 electrolyte, respectively. To eliminate the factor of capacity current, the Li_2S_6-free symmetric cells are also tested. As shown in Fig. 6a, the CoS@rGO composite displays a much higher current density than that of pure rGO, indicating dynamically improved kinetics of redox conversion of polysulfides. Meanwhile, electrochemical impedance spectroscopy (EIS) after CV test is also performed to explore the catalytic capability of CoS by symmetric cells under the frequency range from 200 kHz to 10 mHz at 10.0 mV of sinus amplitude. The semicircular diameter in the Nyquist plots is related with the charge transfer resistance at the electrode/electrolyte with polysulfide interfaces. Fig. 6b shows that the symmetric cell with CoS@rGO electrodes has much lower charge transfer resistance than that with rGO, confirming significantly improved the redox kinetics of polysulfides due to the catalytic effect of CoS on the redox reaction of S/Li_2S. Furthermore, Li-S batteries with rGO/S and CoS/S electrodes are operated by CV at 0.1 mV s^{-1}. The CV curves of the electrodes all exhibit two pairs of redox peaks, *i.e.* the cathodic peaks at 2.29 V and 2.04 V correspond to rGO/S electrode while those at 2.31 V and 2.06 V to CoS/S, and the anodic peaks at 2.34 V and 2.38 V belong to rGO/S electrode while those at 2.31 V and 2.37 V to CoS (Fig. 6c and Fig. S5). In comparison with the redox peaks voltage of rGO/S electrode, CoS/S electrode exhibits higher reducing potential and lower oxidizing potential, indicating that CoS is a key role in enhancing the kinetics of polysulfides conversion.

In addition, the sulfur-host with high conductivity is also very important for the electrochemical performance improvement of Li-S batteries. The resistance of fresh CoS/S, rGO/S and CoS@rGO/S electrodes under the same open circuit voltage (2.4 V) were also tested by EIS with the frequency range from 100 kHz to 10 mHz at 10.0 mV of sinus

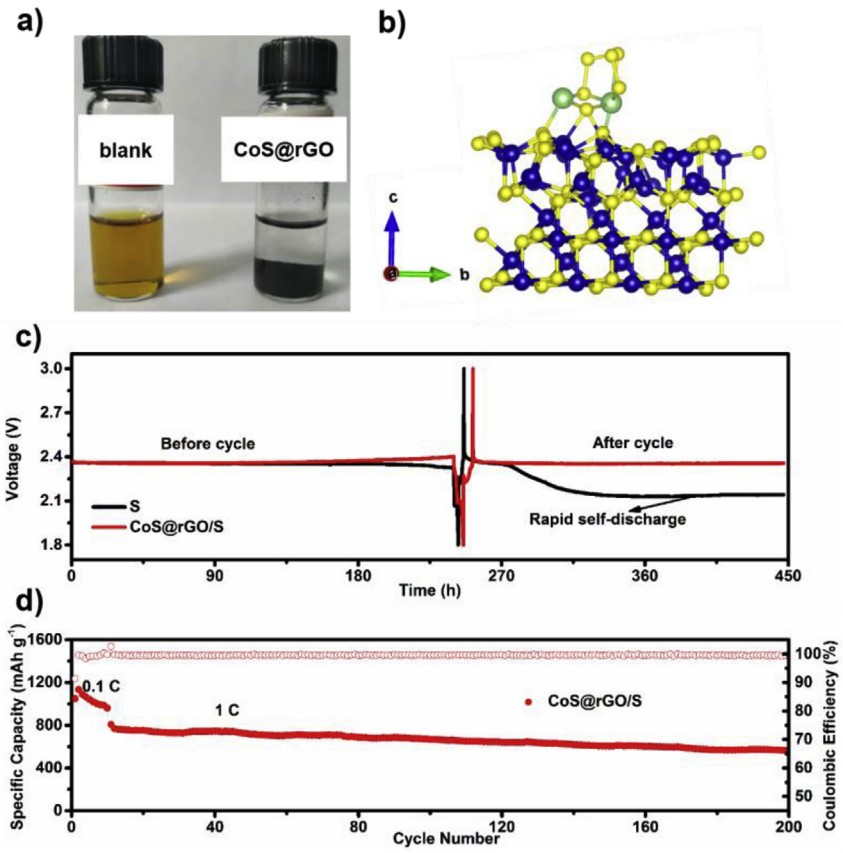

Fig. 5. a) Optical photos of blank and CoS@rGO powders soaked in Li_2S_6-DME solution. b) Relaxed Li_2S_6-adsorbed structures on (101) surface of CoS calculated with density functional theory (DFT). Blue atoms stand for Co, yellow for S, and green for Li. c) The open-circuit voltage of batteries with S and CoS@rGO/S before and after 1st cycle. d) Cycling performance and corresponding Columbic efficiency of the S and CoS@rGO/S electrodes at the current density of 1C. (For interpretation of the references to color in this figure legend, the reader is referred to the Web version of this article.)

amplitude. The Nyquist plots are composed of a semicircle related to the charge transfer resistance and a straight line representing the mass transfer process, as demonstrated in Fig. 6d. The charge transfer resistance of CoS@rGO/S electrode is between that of CoS/S and rGO/S electrodes, indicating its higher conductivity than CoS/S. Then, the rate performances of the CoS@rGO/S, CoS/S and rGO/S electrodes were tested from 0.1 C to 2 C under the voltage window between 1.8 V and 3 V. Indeed, the CoS@rGO/S electrode showed a much better rate performance than CoS/S and rGO/S electrodes due to synergistic effect of high conductivity and catalysis effect. Initially, the CoS@rGO/S electrode displays a high discharge specific capacity about 1161.6 mAh g^{-1} at 0.1 C. When the current density increased to 0.2 C, 0.5 C, 1 C and 2 C, the discharge specific capacities still remained at 897.4, 777.4, 691.5 and 602.0 mAh g^{-1}, respectively. When the cycling rate is reduced back to 0.2 C, the discharge specific capacity is recovered to 786.6 mAh g^{-1}, suggesting the good stability of CoS@rGO/S composite. Moreover, Fig. 6f and Fig. S6 show the charge and discharge voltage curves of the samples at different current rates. The lower voltage gap of CoS@rGO/S (130 mV) than that of rGO/S (151 mV) and CoS/S (140 mV) could also be attributed to the catalytic effect, the better

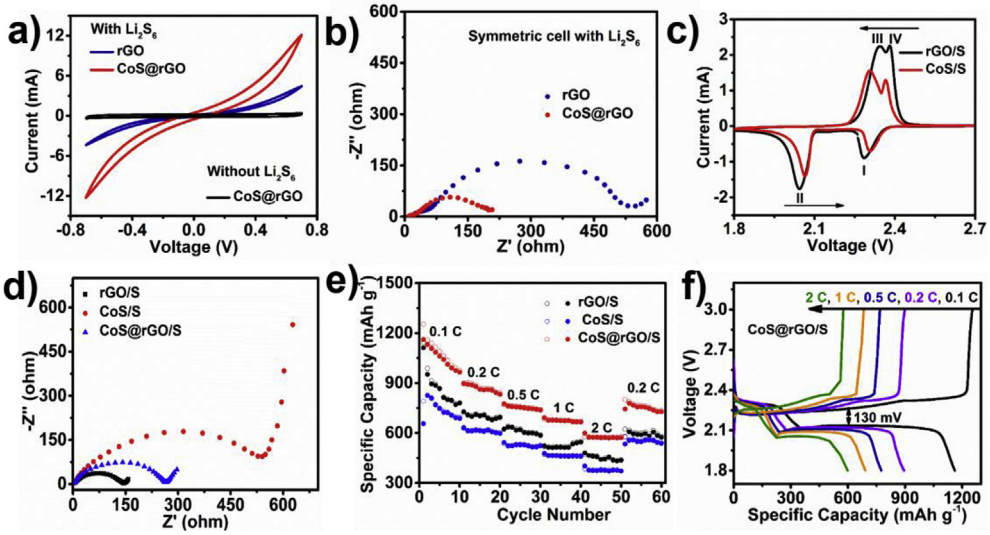

Fig. 6. a) CV curves of symmetric cells. b) EIS data of symmetric Li_2S_6-Li_2S_6 cells. c) CV curves of rGO/S and CoS/S electrodes at a scan rate of 0.1 mV s^{-1}. d) EIS spectra of rGO/S, CoS/S and CoS@rGO/S cathodes. e) Rate performance and f) charge and discharge curves of CoS@rGO/S at different current densities.

conductivity, the small size of nano particles and the high surface area. This contributes to higher energy density and improved rate performance of Li–S batteries. In a word, the introduction of CoS can not only suppress the shuttle effect but also accelerate the kinetics of redox conversion of polysulfides to enhance the electrochemical performances of Li–S batteries.

4. Conclusion

In this work, a trifunctional CoS@rGO composite as sulfur host material was designed and synthesized by a one-step hydrothermal method for performance enhanced Li-S battery. Both the experimental results and theoretical calculations show that there are strong polar–polar interaction between CoS and polysulfides. It also could serve as a catalyst to accelerate the kinetics of redox conversion for polysulfides. In addition, benefiting from the high conductivity of rGO, the composite could improve the utilization of active sulfur and thus significantly improve both the cycling stability and rate performance of Li-S batteries with CoS@rGO electrode. Therefore, the CoS@rGO/S cathode exhibited low self-discharge, good cycling stability, and high rate performance for 602.0 mAh g^{-1} at 2 C. All results manifest the sulfur host materials with abundant polar, catalytic site and high conductivity are key to the design and fabrication of the high-performance of Li–S batteries.

Acknowledgements

The project was supported by the National Natural Science Foundation of China (51702155, 11604235, 21727808, 21574065, 21604038), the Jiangsu Provincial Founds for Natural Science Foundation (BK20170975, BK20160975), the National Science Foundation for Distinguished Young Scholars (21625401), the Program for Outstanding Young Scholars from the Organization Department of the CPC Central Committee and the National Key R&D Program of China (Grant No. 2017YFA0207202 and 2017YFA0207201).

Appendix A. Supplementary data

Supplementary data to this article can be found online at https://doi.org/10.1016/j.jpowsour.2019.03.015.

References

[1] P.G. Bruce, S.A. Freunberger, L.J. Hardwick, J.M. Tarascon, Li-O2 and Li-S batteries with high energy storage, Nat. Mater. 11 (2012) 19–29.
[2] A. Manthiram, S.-H. Chung, C. Zu, Lithium-sulfur batteries: progress and prospects, Adv. Mater. 27 (2015) 1980–2006.
[3] Y.-X. Yin, S. Xin, Y.-G. Guo, L.-J. Wan, Lithium-sulfur batteries: electrochemistry, materials, and prospects, Angew. Chem. Int. Ed. 52 (2013) 13186–13200.
[4] S. Rehman, K. Khan, Y. Zhao, Y. Hou, Nanostructured cathode materials for lithium-sulfur batteries: progress, challenges and perspectives, J. Mater. Chem. 5 (2017) 3014–3038.
[5] S. Urbonaite, T. Poux, P. Novak, Progress towards commercially viable Li-S battery cells, Adv. Energy Mater. 5 (2015) 1500118.
[6] M. Hagen, D. Hanselmann, K. Ahlbrecht, R. Maca, D. Gerber, J. Tubke, Lithium-sulfur cells: the gap between the state-of-the-art and the requirements for high energy battery cells, Adv. Energy Mater. 5 (2015) 1401986.
[7] A. Manthiram, Y.Z. Fu, S.H. Chung, C.X. Zu, Y.S. Su, Rechargeable lithium-sulfur batteries, Chem. Rev. 114 (2014) 11751–11787.
[8] Z. Cui, C. Zu, W. Zhou, A. Manthiram, J.B. Goodenough, Mesoporous titanium nitride-enabled highly stable lithium-sulfur batteries, Adv. Mater. 28 (2016) 6926–6931.
[9] B.-C. Yu, J.-W. Jung, K. Park, J.B. Goodenough, A new approach for recycling waste rubber products in Li-S batteries, Energy Environ. Sci. 10 (2017) 86–90.
[10] X.L. Ji, K.T. Lee, L.F. Nazar, A highly ordered nanostructured carbon-sulphur cathode for lithium-sulphur batteries, Nat. Mater. 8 (2009) 500–506.
[11] Z. Li, J. Zhang, B. Guan, D. Wang, L.M. Liu, X.W. Lou, A sulfur host based on titanium monoxide@carbon hollow spheres for advanced lithium-sulfur batteries, Nat. Commun. 7 (2016) 13065.
[12] C. Hu, H. Chen, Y. Shen, D. Lu, Y. Zhao, A.H. Lu, X. Wu, W. Lu, L. Chen, In situ wrapping of the cathode material in lithium-sulfur batteries, Nat. Commun. 8 (2017) 479.
[13] S. Bai, X. Liu, K. Zhu, S. Wu, H. Zhou, Metal–organic framework-based separator for lithium–sulfur batteries, Nat. Energy 1 (2016) 16094.
[14] M. Li, Y. Wan, J.-K. Huang, A.H. Assen, C.-E. Hsiung, H. Jiang, Y. Han, M. Eddaoudi, Z. Lai, J. Ming, L.-J. Li, Metal–organic framework-based separators for enhancing Li–S battery stability: mechanism of mitigating polysulfide diffusion, ACS Energy Lett 2 (2017) 2362–2367.
[15] L. Qie, W.M. Chen, Z.H. Wang, Q.G. Shao, X. Li, L.X. Yuan, X.L. Hu, W.X. Zhang, Y.H. Huang, Nitrogen-doped porous carbon nanofiber webs as anodes for lithium ion batteries with a superhigh capacity and rate capability, Adv. Mater. 24 (2012) 2047–2050.
[16] T.Z. Zhuang, J.Q. Huang, H.J. Peng, L.Y. He, X.B. Cheng, C.M. Chen, Q. Zhang, Rational integration of polypropylene/graphene oxide/nafion as ternary-layered separator to retard the shuttle of polysulfides for lithium-sulfur batteries, Small 12 (2016) 381–389.
[17] G. Li, M. Ling, Y. Ye, Z. Li, J. Guo, Y. Yao, J. Zhu, Z. Lin, S. Zhang, Acacia Senegal-inspired bifunctional binder for longevity of lithium-sulfur batteries, Adv. Energy Mater. 5 (2015) 1500878.
[18] M. Ling, L. Zhang, T. Zheng, J. Feng, J. Guo, L. Mai, G. Liu, Nucleophilic substitution between polysulfides and binders unexpectedly stabilizing lithium sulfur battery, Nanomater. Energy 38 (2017) 82–90.
[19] J. Liu, D.G.D. Galpaya, L. Yan, M. Sun, Z. Lin, C. Yan, C. Liang, S. Zhang, Exploiting a robust biopolymer network binder for an ultrahigh-areal-capacity Li–S battery, Energy Environ. Sci. 10 (2017) 750–755.
[20] L. Zhang, M. Ling, J. Feng, G. Liu, J. Guo, Effective electrostatic confinement of polysulfides in lithium/sulfur batteries by a functional binder, Nanomater. Energy 40 (2017) 559–565.
[21] G.G. Eshetu, X. Judez, C.M. Li, O. Bondarchuk, L.M. Rodriguez-Martinez, H. Zhang, M. Armand, Lithium azide as an electrolyte additive for all-solid-state lithium-sulfur batteries, Angew. Chem. Int. Ed. 56 (2017) 15368–15372.
[22] H. Dai, K. Xi, X. Liu, C. Lai, S. Zhang, Cationic surfactant based electrolyte additives for uniform lithium deposition via lithiophobic repulsion mechanisms, J. Am. Chem. Soc. 50 (2018) 17515–17521.
[23] S. Li, H. Dai, Y. Li, C. Lai, J. Wang, F. Huo, C. Wang, Designing Li-protective layer via SOCl2 additive for stabilizing lithium-sulfur battery, Energy Storage Materials (2018), https://doi.org/10.1016/j.ensm.2018.09.012.
[24] L.-X. Miao, W.-K. Wang, A.-B. Wang, K.-G. Yuan, Y.-S. Yang, A high sulfur content composite with core-shell structure as cathode material for Li-S batteries, J. Mater. Chem. 1 (2013) 11659–11664.
[25] M.-Q. Zhao, M. Sedran, Z. Ling, M.R. Lukatskaya, O. Mashtalir, M. Ghidiu, B. Dyatkin, D.J. Tallman, T. Djenizian, M.W. Barsoum, Y. Gogotsi, Synthesis of carbon/sulfur nanolaminates by electrochemical extraction of titanium from Ti2SC, Angew. Chem. Int. Ed. 54 (2015) 4810–4814.
[26] D. Yang, W. Ni, J.L. Cheng, Z.P. Wang, T. Wang, Q. Guan, Y. Zhang, H. Wu, X.D. Li, B. Wang, Flexible three-dimensional electrodes of hollow carbon bead strings as graded sulfur reservoirs and the synergistic mechanism for lithium-sulfur batteries, Appl. Surf. Sci. 413 (2017) 209–218.
[27] J.J. Song, C.Y. Zhang, X. Guo, J.Q. Zhang, L.Q. Luo, H. Liu, F.Y. Wang, G.X. Wang, Entrapping polysulfides by using ultrathin hollow carbon sphere-functionalized separators in high-rate lithium-sulfur batteries, J. Mater. Chem. 6 (2018) 16610–16616.
[28] H.Y. Gu, R. Zhang, P. Wang, S.M. Xie, C.M. Niu, H.K. Wang, Construction of three-dimensional ordered porous carbon bulk networks for high performance lithium-sulfur batteries, J. Colloid Interface Sci. 533 (2019) 445–451.
[29] G. Hu, C. Xu, Z. Sun, S. Wang, H.-M. Cheng, F. Li, W. Ren, 3D graphene-foam-reduced-graphene-oxide hybrid nested hierarchical networks for high-performance Li-S batteries, Adv. Mater. 28 (2016) 1603–1609.
[30] P. Xiao, F. Bu, G. Yang, Y. Zhang, Y. Xu, Integration of graphene, nano sulfur, and conducting polymer into compact, flexible lithium-sulfur battery cathodes with ultrahigh volumetric capacity and superior cycling stability for foldable devices, Adv. Mater. 29 (2017) 1703324.
[31] X. Liu, J.Q. Huang, Q. Zhang, L.Q. Mai, Nanostructured metal oxides and sulfides for lithium-sulfur batteries, Adv. Mater. 29 (2017) 1601759.
[32] X. Tao, J. Wang, C. Liu, H. Wang, H. Yao, G. Zheng, Z.W. Seh, Q. Cai, W. Li, G. Zhou, C. Zu, Y. Cui, Balancing surface adsorption and diffusion of lithium-polysulfides on nonconductive oxides for lithium-sulfur battery design, Nat. Commun. 7 (2016) 11203.
[33] G. Zhou, H. Tian, Y. Jin, X. Tao, B. Liu, R. Zhang, Z.W. Seh, D. Zhuo, Y. Liu, J. Sun, J. Zhao, C. Zu, D.S. Wu, Q. Zhang, Y. Cui, Catalytic oxidation of Li2S on the surface of metal sulfides for Li-S batteries, Proc. Natl. Acad. Sci. U.S.A. 114 (2017) 840.
[34] Y. Wang, M. Li, L. Xu, T. Tang, Z. Ali, X. Huang, Y. Hou, S. Zhang, Polar and conductive iron carbide@N-doped porous carbon nanosheets as a sulfur host for high performance lithium sulfur batteries, Chem. Eng. J. 358 (2019) 962–968.
[35] Q. Zhang, Y. Zhou, F. Xu, H. Lin, Y. Yan, K. Rui, C. Zhang, Q. Wang, Z. Ma, Y. Zhang, K. Huang, J. Zhu, W. Huang, Topochemical synthesis of 2D carbon hybrids through self-boosting catalytic carbonization of a metal-polymer framework, Angew. Chem. Int. Ed. 57 (2018) 16436–16441.
[36] Y. Wang, D. Adekoya, J. Sun, T. Tang, H. Qiu, L. Xu, S. Zhang, Y. Hou, Manipulation of edge-site Fe–N2 moiety on holey Fe, N codoped graphene to promote the cycle stability and rate capacity of Li–S batteries, Adv. Funct. Mater. (2018) 1807485.
[37] D. Liu, C. Zhang, G. Zhou, W. Lv, G. Ling, L. Zhi, Q.-H. Yang, Catalytic effects in lithium-sulfur batteries: promoted sulfur transformation and reduced shuttle effect, Adv. Sci. (2017) 1700270.
[38] X.Y. Yu, L. Yu, X.W. Lou, Metal sulfide hollow nanostructures for electrochemical energy storage, Adv. Energy Mater. 6 (2016) 1501333.
[39] C. Ye, L. Zhang, C. Guo, D. Li, A. Vasileff, H. Wang, S.-Z. Qiao, A 3D hybrid of chemically coupled nickel sulfide and hollow carbon spheres for high performance

lithium-sulfur batteries, Adv. Funct. Mater. 27 (2017) 1702524.
[40] Z. Yuan, H.-J. Peng, T.-Z. Hou, J.-Q. Huang, C.-M. Chen, D.-W. Wang, X.-B. Cheng, F. Wei, Q. Zhang, Powering lithium-sulfur battery performance by propelling polysulfide redox at sulfiphilic hosts, Nano Lett. 16 (2016) 519–527.
[41] S.-H. Chung, L. Luo, A. Manthiram, TiS_2-polysulfide hybrid cathode with high sulfur loading and low electrolyte consumption for lithium-sulfur batteries, ACS Energy Lett 3 (2018) 568–573.
[42] K. Sun, C.A. Cama, R.A. Demayo, D.C. Bock, X. Tong, D. Su, A.C. Marschilok, K.J. Takeuchi, E.S. Takeuchi, H. Gan, Interaction of FeS_2 and sulfur in Li-S battery system, J. Electrochem. Soc. 164 (2017) A6039–A6046.
[43] M. Shao, Y. Cheng, T. Zhang, S. Li, W. Zhang, B. Zheng, J. Wu, W.-W. Xiong, F. Huo, J. Lu, Designing MOFs-derived FeS2@carbon composites for high-rate sodium ion storage with capacitive contributions, ACS Appl. Mater. Interfaces 10 (2018) 33097–33104.
[44] S. Peng, X. Han, L. Li, Z. Zhu, F. Cheng, M.U. Srinivansan, S. Adams, S. Ramakrishna, Unique cobalt sulfide/reduced graphene oxide composite as an anode for sodium-ion batteries with superior rate capability and long cycling stability, Small 12 (2016) 1359–1368.
[45] Y. Gu, Y. Xu, Y. Wang, Graphene-wrapped CoS nanoparticles for high-capacity lithium-ion storage, ACS Appl. Mater. Interfaces 5 (2013) 801–806.
[46] P. Hohenberg, W. Kohn, Inhomogeneous electron gas, Phys. Rev. 136 (1964) B864–B871.
[47] G. Kresse, J. Furthmuller, Efficient iterative schemes for ab initio total-energy calculations using a plane-wave basis set, Phys. Rev. B 54 (1996) 11169–11186.
[48] G. Kresse, D. Joubert, From ultrasoft pseudopotentials to the projector augmented-wave method, Phys. Rev. B 59 (1999) 1758–1775.
[49] J.P. Perdew, K. Burke, M. Ernzerhof, Generalized gradient approximation made simple, Phys. Rev. Lett. 77 (1996) 3865–3868.
[50] P.E. Blochl, Augmented-wave method, Phys. Rev. B 50 (1994) 17953–17979.
[51] Y. Chen, X. Li, K. Park, L. Zhou, H. Huang, Y.-W. Mai, J.B. Goodenough, Hollow nanotubes of N-doped carbon on CoS, Angew. Chem. Int. Ed. 55 (2016) 15831–15834.
[52] P. Lian, J. Wang, D. Cai, L. Ding, Q. Jia, H. Wang, Porous SnO2@C/graphene nanocomposite with 3D carbon conductive network as a superior anode material for lithium-ion batteries, Electrochim. Acta 116 (2014) 103–110.
[53] G. Zhou, E. Paek, G.S. Hwang, A. Manthiram, Long-life Li/polysulphide batteries with high sulphur loading enabled by lightweight three-dimensional nitrogen/sulphur-codoped graphene sponge, Nat. Commun. 6 (2015) 7760.
[54] L. Luo, S.H. Chung, A. Manthiram, Rational design of a dual-function hybrid cathode substrate for lithium-sulfur batteries, Adv. Energy Mater. 8 (2018) 1801014.
[55] I. Alstrup, I. Chorkendorff, R. Candia, B.S. Clausen, H. Topsoe, A combine X-ray photoelectron and mossbauer emission-spectroscopy study of the state cobalt sulfide, supported, and unsupported CO-MO catalysts, J. Catal. 77 (1982) 397–409.
[56] T.I. Koranyi, I. Manninger, Z. Paal, O. Marks, J.R. Gunter, Activation of unsupported CO-MO catalysts in thiophene hydrodesulfurization, J. Catal. 116 (1989) 422–439.
[57] Q. Pang, D. Kundu, L.F. Nazar, A graphene-like metallic cathode host for long-life and high-loading lithium-sulfur batteries, Mater. Horiz. 3 (2016) 130–136.
[58] L. Ma, W. Zhang, L. Wang, Y. Hu, G. Zhu, Y. Wang, R. Chen, T. Chen, Z. Tie, J. Liu, Z. Jin, Strong capillarity, chemisorption, and electrocatalytic capability of criss-crossed nanostraws enabled flexible, high-rate, and long-cycling lithium sulfur batteries, ACS Nano 12 (2018) 4868–4876.
[59] C. Zheng, S. Niu, W. Lv, G. Zhou, J. Li, S. Fan, Y. Deng, Z. Pan, B. Li, F. Kang, Q.-H. Yang, Propelling polysulfides transformation for high-rate and long-life lithium sulfur batteries, Nanomater. Energy 33 (2017) 306–312.
[60] Q. Pang, X. Liang, C.Y. Kwok, J. Kulisch, L.F. Nazar, A comprehensive approach toward stable lithium-sulfur batteries with high volumetric energy density, Adv. Energy Mater. 7 (2017) 1801014.